Modeling and Analysis of a Polyphase Wireless Power Transfer System for EV Charging Applications

Rong Zeng, Omer C. Onar, Mostak Mohammad, Gui-Jia Su, Erdem Asa, and Veda P. Galigekere
Buildings and Transportation Science Division, Energy Science and Technology Directorate
Oak Ridge National Laboratory, Oak Ridge, TN
Emails: zengr@ornl.gov, onaroc@ornl.gov, mohammadm@ornl.gov, sugj@ornl.gov, asae@ornl.gov, galigekerevn@ornl.gov

***Abstract*— Extreme fast charging is an emerging technology targeting to significantly decrease charging times of electric vehicles to 10-20 minutes, similar to an interstate gas refueling practice. High-power wireless power transfer (WPT) systems with polyphase electromagnetic couplers can be an attractive solution for these applications due to the very high surface power density of polyphase coils with reduced ripple current characteristics on both the primary and secondary sides that result in more compact designs with reduced dc bus bar capacitor requirements. In addition, WPT systems offer automated charging process, which can be an enabling technology for connected and automated vehicles, with high-efficiency, convenience, safety, and flexibility. This study presents a matrix representation of a mathematical model for a three-phase WPT system with series-series connected three-phase resonant compensation networks. Nonzero interphase mutual inductances between the same side phase windings are considered for tuning to obtain a circuit model for parametric sensitivity. Simulation and experimental results presented for a 50-kW experimental prototype to demonstrate the operation of the polyphase WPT system.**

Keywords*— *polyphase wireless power transfer, electric vehicle, wireless charging, resonance

I. Introduction

As the transportation electrification is accelerating, U.S. Department of Energy published a report to analyze the technology gaps of extreme fast charging for electric vehicles with a power of 350 kW, which is an emerging technology enabling similar refueling experience for electric vehicles (EVs) to that of conventional gasoline vehicles [1]. High-power wireless power transfer (WPT) is a promising candidate for extreme fast charging since it automates the charging process with no driver involvement with the high-power charging equipment [2].

Many studies on WPT systems have been conducted in single-phase type of couplers [3], [4]. Since the power rating of WPT system increases, polyphase WPT systems have drawn wide attention because of its superiorities in achieving higher power transfer capability and reducing the size of transmitter and receiver coils for a given power rating. Moreover, polyphase couplers provide a more uniform magnetic field distribution, allowing better utilization of allocated space, and achieve a smooth power transfer [5] with reduced voltage and current ripples both at the input and output [6], [7].

While most of the previous studies use non-rotating electromagnetic fields in three-phase coil arrangements, this study focuses on the modeling and experimental validation of a two-layer, three-phase system with rotating magnetic fields on spatially phase-shifted windings that are electrically excited with voltages that are also 120° phase-shifted. The bipolar two-layer three-phase WPT coil structure is presented in Fig. 1. Basically, the coil coupler consists of three winding pairs. Each pair includes two windings with opposite polarity. Additionally, while most of the previous studies tried to eliminate or reduce the interphase cross-couplings (mutual inductances between same side phase windings), this study uses non-zero interphase mutual inductances. Since the physical rotation of the phase windings is >90°, the interphase mutual inductances are negative which implies that the mutual coupling between the phases increase the power transfer, resulting in higher utilization of the coupler surface area.

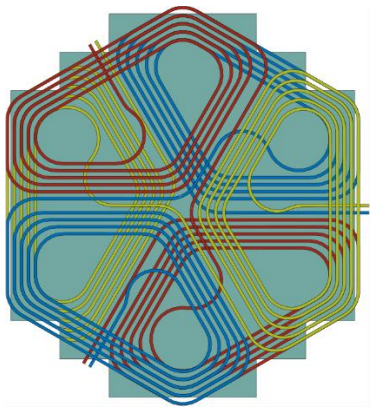

Fig. 1. Bipolar two-layer three-phase WPT coil structure.

In the literature, there are some existing systems using three-phase approaches although they are fundamentally different from the work proposed here. To reduce power fluctuation in dynamic inductive power transfer system, a three-phase inverter with a three-phase transmitter and a single-phase receiver was proposed in [8] that resulted in a wider power delivery zone than that of the single-phase track layout. A three-phase wireless charging system for underwater vehicles was proposed in [9].

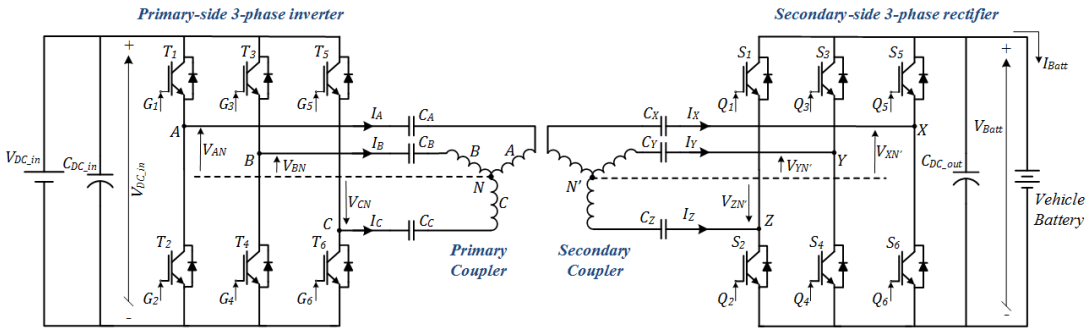

Fig. 2. Circuit diagram of the proposed system.

with spatially 120° phase shifted solenoid transmitters and receivers for up to 1.2 kW power transfer levels. Reference [10] presented theory and analysis of three-phase inductive WPT systems with bipolar phase windings and discussed magnetic coupler topologies and the theoretical and practical aspects of series-series connected three-phase resonant compensation networks. In [11], a three-phase dynamic wireless charging system was studies with reduced leakage magnetic fields whereas [12] presented the analysis and design of a multiphase receiver configuration for the reduction of output power pulsations for a dynamic wireless charging system. A four-coil WPT system was studied in [13] with a tripolar pad-based transmitter and a single-phase receiver with non-rotating magnetic fields for up to 3.3 kW power transfer level. Magnetic modeling of a three-phase WPT system was presented in [14] with three circular unipolar coils for up to 10 kW design target.

Rest of the paper is organized as follows: Section II presents the inductance matrix of the proposed polyphase coupler system with current dependent voltage source model of the interphase couplings along with the matrix representation of the system equation. Section III introduces the simulation model and the simulation results. Section IV presents the experimental results along with the power transfer and overall dc-to-dc efficiency on the 50-kW laboratory test setup.

II. System Modeling

The schematic diagram of a three-phase WPT system is illustrated in Fig. 2 which consists of a primary-side dc source and a three-phase high-frequency inverter, three-phase Y-Y connected coupling coils with their series-series connected capacitive compensation network, a secondary-side three-phase rectifier, a filter capacitor, and connection to the battery load.

The equivalent circuit of three-phase WPT system with nonzero interphase mutual inductance is shown in Fig. 3. V_{AN}, V_{BN} and V_{CN} are the phase-to-neutral output voltage of primary-side inverter, and the amplitude can be express as

$$\left|\dot{V_{AN}}\right| = \left|\dot{V_{AN}}\right| = \left|\dot{V_{AN}}\right| = \frac{\sqrt{2}}{\pi} V_{DC_{in}} \tag{1}$$

where $V_{DC_{in}}$ is the dc-bus voltage to the inverter input.

Coil currents I_A, I_B, I_C and I_X, I_Y, I_Z flow into the ground coils and vehicle coils, respectively. R_{eq} is the equivalent load resistance representing the vehicle battery load. The equivalent circuit model of this polyphase system, considering all the mutual inductances between primary-side phases, secondary-side phases, and between primary and secondary-side phases is shown in Fig. 3.

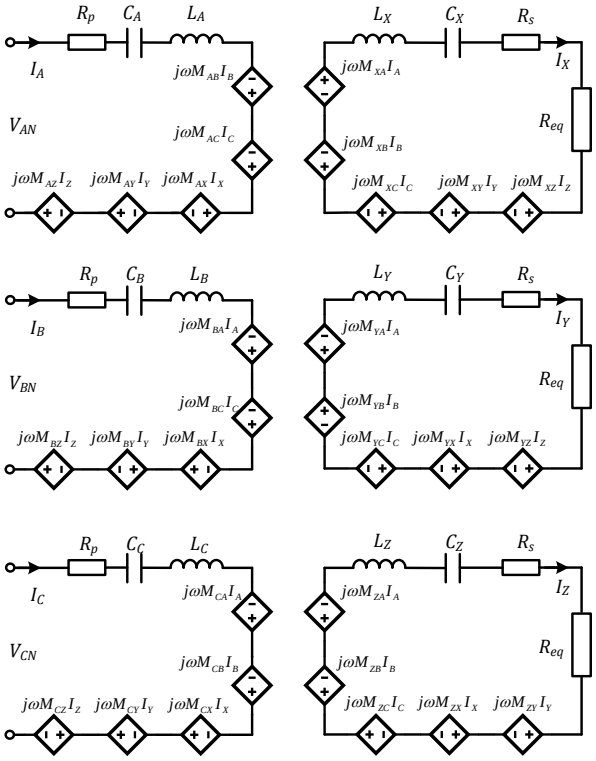

Fig. 3. Three-phase WPT system equivalent circuit model.

The inductance matrix with the self-inductances of each phase windings and all the magnetic couplings between them can be defined by

$$L = \begin{bmatrix} L_A & M_{AB} & M_{AC} & M_{AX} & M_{AY} & M_{AZ} \\ M_{BA} & L_B & M_{BC} & M_{BX} & M_{BY} & M_{BZ} \\ M_{CA} & M_{CB} & L_C & M_{CX} & M_{CY} & M_{CZ} \\ M_{XA} & M_{XB} & M_{XC} & L_X & M_{XY} & M_{XZ} \\ M_{YA} & M_{YB} & M_{YC} & M_{YX} & L_Y & M_{YZ} \\ M_{ZA} & M_{ZB} & M_{ZC} & M_{ZX} & M_{ZY} & L_Z \end{bmatrix} \tag{2}$$

where L_A, L_B, and L_C are the primary-side phase self-inductances, L_X, L_Y, and L_Z are the secondary-side phase self-inductances, M_{AB}=M_{BA}, M_{AC}=M_{CA}, and M_{BC}=M_{CB} are the mutual inductances between primary-side phase windings, M_{XY}=M_{YX}, M_{XZ}=M_{ZX}, and M_{YZ}=M_{ZY} are the secondary-side mutual inductances between secondary-side phase windings,

and M_{AX}=M_{XA}, M_{AY}=M_{YA}, M_{AZ}=M_{ZA}, M_{BX}=M_{XB}, M_{BY}=M_{YB}, M_{BZ}=M_{ZB}, and M_{CX}=M_{XC}, M_{CY}=M_{YC}, M_{CZ}=M_{ZC} are the mutual inductances between all the primary and secondary-side phase windings. The inductance matrix in (2) is diagonally symmetric under ideal conditions.

In this polyphase coupler design, complex power expression is given by

$$S = j\omega I_p^H M_{PS} I_S \tag{3}$$

where I_P is the vector of primary currents (RMS), I_S is the vector of secondary currents (RMS), M_{PS} is the mutual inductance matrix between all primary and all secondary phases, and $()^H$ denotes the complex conjugate transpose. Active power transfer is the real part of this power expression in complex domain and can be written by:

$$P = \Re eal(S). \tag{4}$$

In a perfectly aligned, balanced three-phase system, primary-side and secondary-side currents are:

$$I_P = I\begin{bmatrix} 1 \\ e^{\frac{j2\pi}{3}} \\ e^{-\frac{j2\pi}{3}} \end{bmatrix} \text{ and } I_S = j[I_P] \tag{5}$$

The mutual inductance matrix representing the magnetic coupling between the primary windings and secondary windings is described by:

$$M_{PS} = \begin{bmatrix} M_{AX} & M_{BX} & M_{CX} \\ M_{AY} & M_{BY} & M_{CY} \\ M_{AZ} & M_{BZ} & M_{CZ} \end{bmatrix} \tag{6}$$

The primary-to-secondary magnetic coupling matrix determines the power transfer; most of the power is transferred between phase A and X, B and Y, and C and Z with positive and ideally identical mutual inductances between these phases (M=M_{AX}≈M_{BY}≈M_{CZ}>0). All other mutual inductances (i.e., which can be denoted by M_k) are negative both in (2) and (6) since the physical rotations of the phases are >90°. This implies that M-M_k>M; therefore, negative mutual couplings between phases increase the power transfer which further contributes to higher surface power densities in polyphase coupler designs. It should also be noted that this polyphase coupler design is independent of any rotational misalignments since all phases would rotate by the same θ angle which converts the mutual inductance in (6) into a circulant structure.

According to Fig. 3, voltage and current equations can be derived based on the impedances and "*current controlled voltage source*" based representation of the mutual inductance related voltage drops or increases. For example, for phase A on primary-side and for phase X on secondary-side, voltage equations are:

$$V_{AN} = \left(R_p + \frac{1}{j\omega C_A} + j\omega L_A\right) I_A + j\omega(-M_{AB}I_B - M_{AC}I_C + M_{AX}I_X - M_{AY}I_Y - M_{AZ}I_Z) \tag{7}$$

$$0 = -\left(R_S + \frac{1}{j\omega C_X} + j\omega L_X + R_{eq}\right) I_X + j\omega(M_{XA}I_A - M_{XB}I_B - -M_{XC}I_C - M_{XY}I_Y - M_{XZ}I_Z) \tag{8}$$

Similar equations can be derived for other phases and these equations can be generalized into a matrix structure that includes all the voltages, currents, tuning network impedances, and self-inductances of all the phase windings, and the mutual inductances between all phases as

$$\begin{bmatrix} V_{AN} \\ V_{BN} \\ V_{CN} \\ 0 \\ 0 \\ 0 \end{bmatrix} = \begin{bmatrix} Z_A & j\omega M_{AB} & j\omega M_{AC} & j\omega M_{AX} & j\omega M_{AY} & j\omega M_{AZ} \\ j\omega M_{BA} & Z_B & j\omega M_{BC} & j\omega M_{BX} & j\omega M_{BY} & j\omega M_{BZ} \\ j\omega M_{CA} & j\omega M_{CB} & Z_C & j\omega M_{CX} & j\omega M_{CY} & j\omega M_{CZ} \\ j\omega M_{XA} & j\omega M_{XB} & j\omega M_{XC} & -Z_X & j\omega M_{XY} & j\omega M_{XZ} \\ j\omega M_{YA} & j\omega M_{YB} & j\omega M_{YC} & j\omega M_{YX} & -Z_Y & j\omega M_{YZ} \\ j\omega M_{ZA} & j\omega M_{ZB} & j\omega M_{ZC} & j\omega M_{ZX} & j\omega M_{ZY} & -Z_Z \end{bmatrix} \begin{bmatrix} I_A \\ I_B \\ I_C \\ I_X \\ I_Y \\ I_Z \end{bmatrix} \tag{9}$$

where $Z_i = R_p + j\omega L_i + 1/j\omega C_i$, $(i = A, B, C)$ denotes the primary-side impedances and $Z_j = R_s + j\omega L_j + 1/j\omega C_j + R_{eq}$, $(j = X, Y, Z)$ denotes the secondary-side impedances and R_{eq} is the equivalent per-phase load resistance. For a three-phase diode bridge rectifier, depending on the battery voltage and the output power, this equivalent resistance can be expressed by

$$R_{eq} = \frac{(\pi V_{batt})^2}{18P_o}. \tag{10}$$

Based on the matrix equation (9), the output phase currents can be generalized and calculated by

$$I_j = \frac{\sum j\omega MI}{Z_j}. \tag{11}$$

Input and output power of this system can be expressed by:

$$P_{in} = V_{AN}I_A cos\varphi_A + V_{BN}I_B cos\varphi_B + V_{CN}I_C cos\varphi_C \tag{12}$$

$$P_{out} = (I_X^2 + I_Y^2 + I_Z^2)R_{eq} \tag{13}$$

For determining the resonant tuning capacitor values, detailed derivations are presented in [10] which implies that only the primary-side self and mutual inductances considered for tuning. In practice, first the equivalent inductance that needs to be compensated should be calculated by

$$L' = L - M \tag{14}$$

For phase A, this expression is then:

$$L'_A = L_A - M_{AB} + M_{BC} - M_{AC} \tag{15}$$

Finally, the tuning capacitor for phase A is

$$C_A = \frac{1}{\omega^2 L'_A} \tag{16}$$

and the tuning capacitor values for other phases can be calculated similarly.

III. Simulation Results

A simulation model using the designed polyphase coupling coils parameters is developed in Plexim/PLECS, as shown in Fig. 4. In this model, polyphase coupling coils is represented by a 6-by-6 inductance matrix, as written in (2), with the measured values of the self-inductances of all the phase windings as well as the mutual inductances between all the phases. The simulation model shown in Fig. 4 includes a three-phase inverter on the primary-side, a three-phase rectifier on the secondary-side, coupled inductor model of the Y connected polyphase couplers

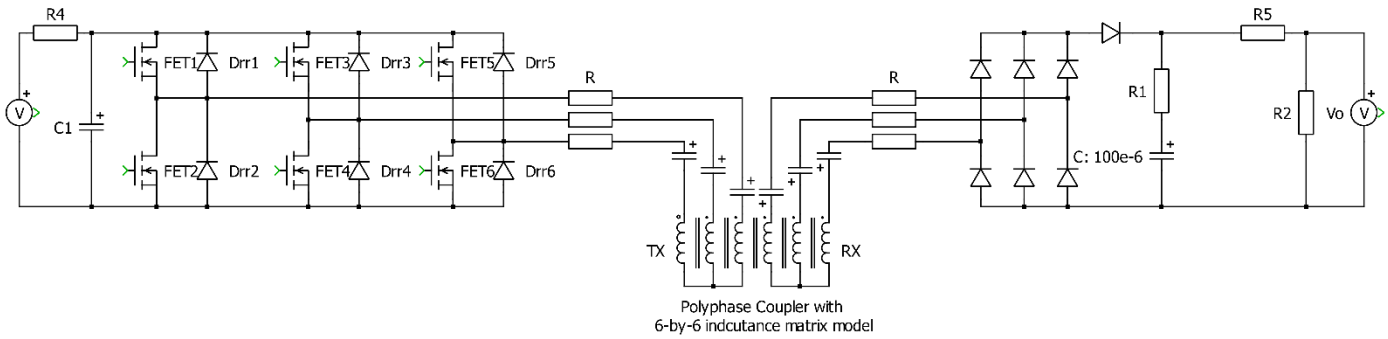

Fig. 4. Simulation model developed in PLECS.

represented by the inductance matrix, and their series connected resonant tuning capacitors for each phase windings. Inductance matrix based on the experimental measurement values is given by:

$$L = \begin{bmatrix} 34.1 & -11.2 & -11.1 & -5.65 & -1.85 & -3.64 \\ -11.2 & 34.3 & -11.3 & -3.64 & 5.54 & -1.77 \\ -11.1 & -11.3 & 34.2 & -1.85 & -3.57 & 5.55 \\ 5.65 & -3.64 & -1.85 & 34.1 & -11.2 & -11.1 \\ -1.85 & 5.54 & -3.57 & -11.2 & 34.3 & -11.3 \\ -3.64 & -1.77 & 5.55 & -11.1 & -11.3 & 34.2 \end{bmatrix} \quad (17)$$

The additional parameters used in the simulation model is listed in Table I.

TABLE I. SIMULATION MODEL PARAMETERS

Parameter	Value	Unit
Target power	50	[kW]
Nominal switching frequency	85	[kHz]
DC bus filter rcapacitors	100	[µF]
Primary and secodary side tuning capacitors	90.7	[nF]
Load resistance after three-phase rectifier	7	[Ω]

The inverter in this simulation model is controlled in an open-loop fashion with a fixed switching frequency and duty cycle with 120 degrees of phase difference between each output phases. Input dc bus voltage to the primary side inverter is set to 556 V to match the experimental results detailed in Section IV. Primary-side phase-to-phase voltages and phase currents are provided in Fig. 5. Due to the slight differences in phase winding self-inductances and the asymmetries between the mutual inductances, phase currents are also slightly imbalanced. In Fig. 6, simulation results of secondary-side phase-to-phase voltages and currents are presented. Similar line current imbalances exist in secondars-side currents although the imbalance in amplitudes is reasonably low and does not cause any considerable issues on the operation of the inverter, rectifier, and the coupling coils. Inverter input voltage and current as well as the rectifier output voltage and current are given in Fig. 7. While the input dc voltage is set to 556 V, output voltage after the rectifier is 592 V, input current is 94.4 A, and the output load current is 84.6 A in steady-state conditions. Accordingly, the input dc power was ~52.63 kW and output dc power was ~50.12 kW, which results in a dc-to-dc efficiency of 95.2%. Simulation results show that the polyphase couplers with 6-by-6 inductance matrix can perform well and achieve the target power transfer rate with high efficiency.

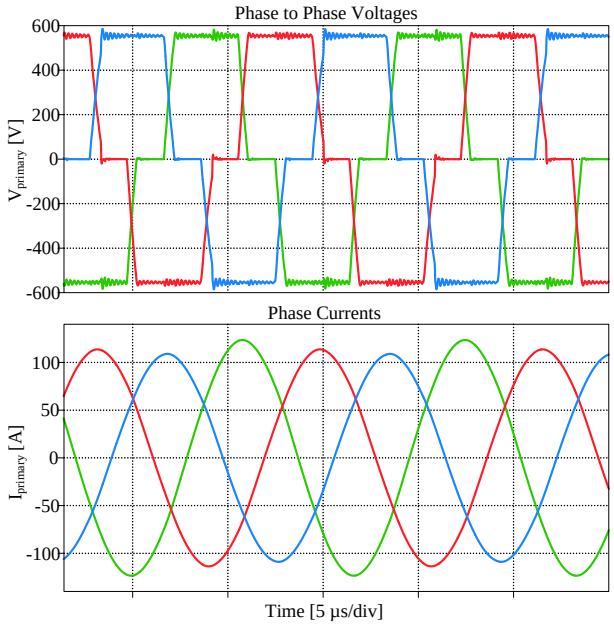

Fig. 5. Primary-side phase-to-phase voltages and line currents.

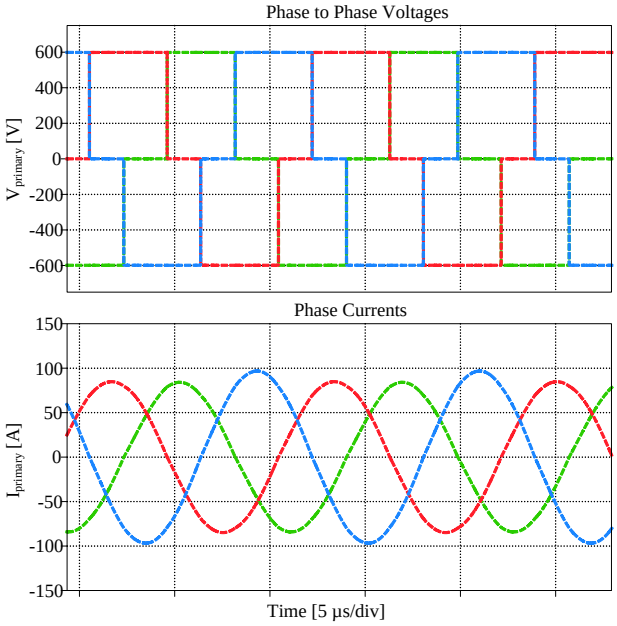

Fig. 6. Secondary-side phase-to-phase voltages and line currents.

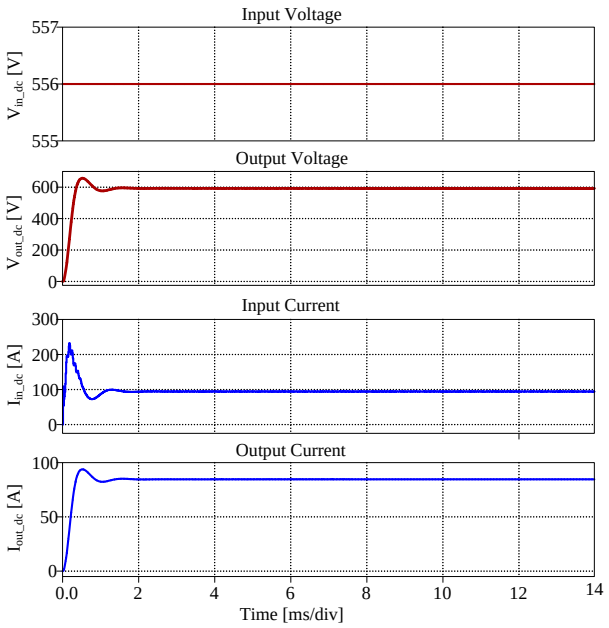

Fig. 7. Input and output dc voltages and currents.

IV. Experimental Results

The prototype development of the proposed identical polyphase transmitter and receiver coupling coils is shown in Fig. 8 with 170mm ground clearance (distance from secondary side coil surface to the ground). The bounding box dimensions of hexagonal shaped couplers is 47.1×54.4 cm and the total weight of each coupler is 13.7 kg which is considered to be a very lightweight design for 50 kW rated power. The 6 AWG Litz wire used in this design is a product of New England Wire and utilizes strand gauge of 38 AWG. Ferrite backplate uses 5 mm thick PLT64/50/5 ferrite tiles made of 3C94 material.

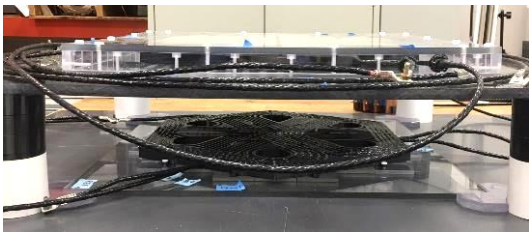

Fig. 8. Hardware realization of the 3-phase polyphase electromagnetic couplers.

The three-phase high-frequency inverter developed for this study is shown in Fig. 9. This inverter development uses the 1200 V / 256 A rated (@125°C case and 175°C junction temperature conditions) Wolfspeed/CREE CAS325M12HM2 SiC MOSFET half-bridge power modules with 3.7 mΩ on-state resistance. Gate drivers are CGD15HB62LP from the same manufacturer. The heatsink is CP3009 liquid cooled cold plate from MicroCool. Inverter also uses two 947D601K901DCRSN 900V / 600 µF rated film capacitors in addition to the 3 µF SCD305K122C3Z25-F snubber capacitors on each power module. Finally, inverter is controlled with a TMS320F28335PGFA DSP from Texas Instruments. Inverter is controlled in an open-loop configuration for the laboratory validation purposes. The experimental test setup with the three-phase inverter and rectifier and the polyphase coupling coils is shown in Fig. 10 where the primary-side inverter is fed with an NHR 9300 dc emulator in dc power supply mode and rectifier output is connected to an additional NHR 9300 dc emulator in dc load mode in parallel with a 14 Ω resistor bank.

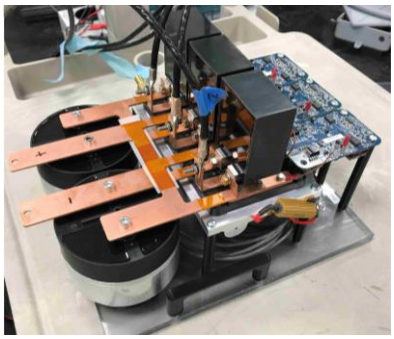

Fig. 9. Three-phase SiC inverter prototype.

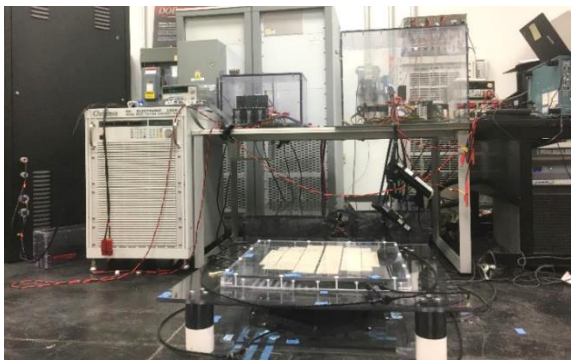

Fig. 10. Experimental test setup.

For the inverter output and rectifier input voltages and currents, a Yokogawa PX8000 high precision power analyzer is used in two-wattmeter method for data recording. Primary-side phase-to-phase voltages V_{AC} and V_{BC} and line currents of I_A and I_B are shown in Fig. 11. This figure also shows the secondary-side phase-to-phase voltages V_{XZ} and V_{YZ} and line currents of I_X and I_Y.

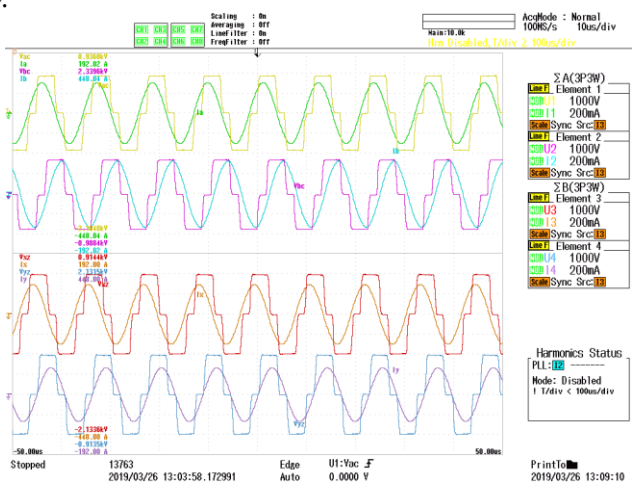

Fig. 11. Primary and secondary-side phase-to-phase voltages V_{AC}, V_{BC}, V_{XZ}, and V_{YZ} and line currents I_A, I_B, I_X, and I_Y.

Moreover, a Yokogawa WT1806E power analyzer is used to measure and record the dc input and output voltage, current, and

power, and the overall input-output (dc-to-dc) efficiency of the system. The input and output dc voltages and currents are shown in Fig. 12 while Fig. 13 shows the numeric recordings of these input and output voltages and currents in addition to the input and output power levels and the dc-to-dc efficiency. As shown in Fig. 13, input power is 52.6 kW, and the output power is 50 kW, and dc-to-dc efficiency is about 95% at this 50-kW operating point. Both the input and output voltage, current, and power levels are closely matching the simulation results, demonstrating the accuracy of the developed model.

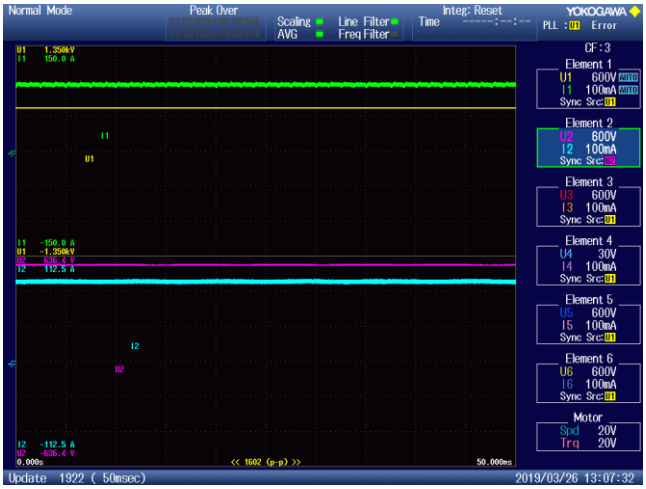

Fig. 12. Inverter input and rectifier output dc voltage and current waveforms.

Fig. 13. Inverter input and rectifier output dc voltage and current waveforms.

V. Conclusions

Modeling and analysis of a three-phase WPT system is presented in this paper, including a three-phase high-frequency inverter and a rectifier with series connected resonant tuning capacitors. Nonzero interphase mutual inductances between the primary and secondary coils are considered to obtain a circuit model represented in matrix form. Simulation model based on the 6-by-6 inductance matrix developed and experimentally validated at 50 kW power level. Experimental results closely matched the simulation results based on the model developed. Future research includes analyzing the parametric sensitivity of the polyphase electromagnetic coupler based WPT system.

Acknowledgment

This research used the resources available at the Power Electronics and Electric Machinery Research Center at the National Transportation Research Center, a US Department of Energy (DOE) Office of Energy Efficiency and Renewable Energy user facility operated by the Oak Ridge National Laboratory (ORNL). The authors would like to thank Dr. Burak Ozpineci (ORNL) for his managerial support and technical guidance and Lee Slezak (DOE) for funding this work and project guidance.

References

[1] D. Howell et al., Enabling Fast Charging: A Technology Gap Assessment, U.S. Department of Energy, Washington, DC, USA, Oct. 2017.

[2] G. A. Covic and J. T. Boys, “Modern trends in inductive power transfer for transportation applications,” *IEEE Journal of Emerging and Selected Topics in Power Electronincs*, vol. 1, no. 1, pp. 28–41, March 2013.

[3] V. P. Galigekere, O. Onar, J. Pries, S. Zou, Z. Wang, and M. Chinthavali, "Sensitivity analysis of primary-side LCC and secondary-side series compensated wireless charging system," in *Proc., IEEE Transportation Electrification Conference and Expo (ITEC)*, pp. 885-891, June 2018, Long Beach, CA.

[4] R. Zeng, V. P. Galigekere, O. C. Onar, and B. Ozpineci, "Grid integration and impact analysis of high-power dynamic wireless charging system in distribution network," *IEEE Access*, vol. 9, pp. 6746-6755, January 2021.

[5] G. Su, O. C. Onar, J. Pries, and V. P. Galigekere, "Variable duty control of three-phase voltage source inverter for wireless power transfer systems," in *Proc., IEEE Energy Conversion Congress and Exposition (ECCE)*, pp. 2118-2124, September-October 2019, Baltimore, MD.

[6] M. Mohammad, J. L. Pries, O. C. Onar, V. P. Galigekere, G. -J. Su, and J. Wilkins, "Three-Phase LCC-LCC Compensated 50-kW Wireless Charging System with Non-Zero Interphase Coupling," in *Proc., IEEE Applied Power Electronics Conference and Exposition (APEC)*, pp. 456-462, June 2021, Phoenix, AZ.

[7] H. Li, Y. Liu, K. Zhou, Z. He, W. Li, and R. Mai, “Uniform power IPT system with three-phase transmitter and bipolar receiver for dynamic charging,” *IEEE Transactions on Power Electronics*, vol. 34, no. 3, pp. 2013–2017, Mar. 2019.

[8] G. A. Covic, J. T. Boys, M. L. G. Kissin, and H. G. Lu, “A three-phase inductive power transfer system for roadway-powered vehicles,” *IEEE Transactions on Industrial Electronincs*, vol. 54, no. 6, pp. 3370–3378, December 2007.

[9] T. Kan, R. Mai, P. P. Mercier, and C. C. Mi, “Design and analysis of a three phase wireless charging system for lightweight autonomous underwater vehicles,” *IEEE Transactions on Power Electronics*, vol. 33, no. 8, pp. 6622–6632, August 2018.

[10] J. Pries, V. P. N. Galigekere, O. C. Onar, and G. Su, "A 50-kW three-phase wireless power transfer system using bipolar windings and series resonant networks for rotating magnetic fields," *IEEE Transactions on Power Electronics*, vol. 35, no. 5, pp. 4500-4517, May 2020,

[11] M. Kim, H. Kim, D. Kim, Y. Jeong, H. Park, and S. Ahn, “A three-phase wireless-power-transfer system for online electric vehicles with reduction of leakage magnetic fields,” *IEEE Transactions on Microwave Theory and Techniques*, vol. 63, no. 11, pp. 3806–3813, November 2015.

[12] S. Cui, Z. Wang, S. Han, and C. Zhu, “Analysis and design of multiphase receiver with reduction of output fluctuation for EV dynamic wireless charging system,” *IEEE Transactions on Power Electronics*, vol. 34, no. 5, pp. 4112– 4124, May 2019.

[13] S. Kim, G. A. Covic, and J. T. Boys, “Tripolar pad for inductive power transfer systems for EV charging,” *IEEE Transactions on Power Electronics*, vol. 32, no. 7, pp. 5045–5057, July 2017.

[14] D. J. Thrimawithana, U. K. Madawala, A. Francis, and M. Neath, “Magnetic modeling of a high-power three phase bi-directional IPT system,” in *Proc., 37th Annual Conference of IEEE Industrial Electronincs Society*, pp. 1414–1419, November 2011, Melbourne, Australia.